Article

Infrared Photoluminescence of Nd-Doped Sesquioxide and Fluoride Nanocrystals: A Comparative Study

Fulvia Gennari [1], Milica Sekulić [2], Tanja Barudžija [3], Željka Antić [2], Miroslav D. Dramićanin [2] and Alessandra Toncelli [1,4,5,*]

[1] Dipartimento di Fisica, Università di Pisa, Largo B. Pontecorvo 3, 6127 Pisa, Italy; fulvia.gennari@phd.unipi.it
[2] Centre of Excellence for Photoconversion, Vinča Institute of Nuclear Sciences—National Institute of the Republic of Serbia, University of Belgrade, 11001 Belgrade, Serbia; msekulic@vinca.rs (M.S.); zeljkaa@gmail.com (Ž.A.); dramican@vinca.rs (M.D.D.)
[3] Department of Theoretical Physics and Condensed Matter Physics, Vinča Institute of Nuclear Sciences—National Institute of the Republic of Serbia, University of Belgrade, 11001 Belgrade, Serbia; tbarudzija@vinca.rs
[4] Istituto Nanoscienze CNR, Piazza San Silvestro 12, 56127 Pisa, Italy
[5] Istituto Nazionale di Fisica Nucleare-Sezione di Pisa, Largo B. Pontecorvo 3, 56127 Pisa, Italy
[*] Correspondence: alessandra.toncelli@unipi.it; Tel.: +39-050-2214-556

Abstract: Lanthanide ions possess various emission channels in the near-infrared region that are well known in bulk crystals but are far less studied in samples with nanometric size. In this work, we present the infrared spectroscopic characterization of various Nd-doped fluoride and sesquioxide nanocrystals, namely $Nd:Y_2O_3$, $Nd:Lu_2O_3$, $Nd:Sc_2O_3$, $Nd:YF_3$, and $Nd:LuF_3$. Emissions from the three main emission bands in the near-infrared region have been observed and the emission cross-sections have been calculated. Moreover, another decay channel at around 2 μm has been observed and ascribed to the $^4F_{3/2} \rightarrow {}^4I_{15/2}$ transition. The lifetime of the $^4F_{3/2}$ level has been measured under LED pumping. Emission cross-sections for the various compounds are calculated in the 1 μm, 900 nm, and 1.3 μm regions and are of the order of 10^{-20} cm^2 in agreement with the literature results. Those in the 2 μm region are of the order of 10^{-21} cm^2.

Keywords: nanoparticles; infrared spectroscopy; Nd-luminescence

1. Introduction

Lanthanide-doped nanocrystals are widely studied systems for their visible emission features thanks to their unparalleled advantages over other types of materials such as their excellent thermomechanical properties and chemical stability, the large Stokes shift and sharp emission lines, and their long emission lifetimes. In particular, upconverting nanocrystals have received great attention for many different applications in the biomedical field, such as biomedical imaging, drug delivery, and photodynamic therapy [1–3], as well as for thermometric measurements [4,5] and for security applications [6], just to name a few.

Lanthanide ions also possess many efficient near-infrared emission transitions that have been exploited for laser emission in bulk crystals [7]. The possibility to exploit the infrared emission of lanthanide-activated nanocrystals can determine a paradigm shift for some applications and can also open the way to a lot of new types of applications, for example, for deep tissue imaging [8], image-guided surgery [9], and forensic science [10]. For example, nanocrystals with infrared emission have added values for biomedical applications such as the reduction of tissue absorption, light scattering, and autofluorescence. Among the various proposed materials, lanthanide nanocrystals with their intriguing emission properties are among the most promising materials. Moreover, Nd shows some very intense emissions in various infrared regions at around 900 nm, 1064 nm, and 1300 nm. All these emissions come from the decay from the $^4F_{3/2}$ to the lower-lying $^4I_{9/2}$, $^4I_{11/2}$, and

$^4I_{13/2}$ and have been widely exploited even for laser emission, but Nd ions also possess a weaker emission band at around 2 µm that has rarely been observed even in bulk crystals.

Sesquioxides are an important class of oxide crystals that possess good thermal and physical properties, have relatively low phonon energy compared with other oxides, and can be grown to good quality [11]. Unfortunately, the high temperature required for the growth of this class of materials as single crystals (around 2400 °C) makes this process quite demanding [12]. For this reason, the same compositions have been produced in fiber, ceramic, or nanopowder form. Y_2O_3 is probably the most widely studied sesquioxide when doped with Nd as bulk crystal [13], single crystal fiber [14], ceramic [15–17], and nanocrystals [18,19], but also other isomorphs such as Lu_2O_3 [20,21] and Sc_2O_3 [22,23] have shown very interesting emission properties when doped with Nd. In general, the focus of the spectroscopic investigations of these materials is limited to the visible absorption bands and to the main emission channel at around 1 micron, for which there is some inconsistency among the published values of the stimulated emission cross-section, especially when estimated with different techniques. Moreover, Nd also possesses other interesting emission channels at around 900 nm and 1300 nm from which even laser emission has been obtained [14], but very few reports of the emission cross-sections in these regions can be found in the literature. Last but not least, the emission at around 2 µm has never been reported to the best of the authors' knowledge.

Fluoride crystals are considered the preferred choice for emissions in the near-infrared, thanks to their good thermomechanical properties combined with low-phonon energy values, but the bulk crystal growth of this class of materials is complicated due to the high purity needed both for the starting chemicals and for the growth atmosphere.

Synthesis of these materials in nanometric form is accomplished by a polymer complex solution technique (oxides) and a low-temperature, solid-state method (fluorides) to study the infrared emission properties of these materials.

2. Materials and Methods

For syntheses of materials, the following chemicals were used: Y_2O_3 (Alfa Aeser, 99.99%), Sc_2O_3 (Alfa Aeser, 99.99%), Lu_2O_3 (Alfa Aeser, 99.99%), Nd_2O_3 (Alfa Aeser, 99.9%), polyethylene glycol (molecular weight 200, Alfa Aeser), nitric acid (HNO_3, Macron, 65%), and ammonium hydrogen difluoride (NH_4HF_2, Sigma−Aldrich, 98.5%). Nd-doped sesquioxide nanocrystals were prepared by the polymer complex solution method as previously described [24,25]. In brief, the stoichiometric ratio of oxide precursors was dissolved in a hot nitric acid at 130 °C until reaching the completely transparent solution. Then, the polyethylene glycol was added to the solution at a mass ratio of 1:1 to the mass of oxides. The solution was stirred at 80 °C until the nitrate gasses dissipated and a clear gel was formed. The gel was pre-sintered for 2 h at 800 °C in a ceramic crucible to produce a voluminous white powder, which was subsequently formed into pellets and calcined for 24 h at 1100 °C. Nd-doped fluorides were prepared by a low-temperature, solid-state synthesis accompanied by fluorination, as previously described [26]. In brief, the appropriate amounts of oxides were mixed with NH_4HF_2, thoroughly ground in an agate mortar to ensure homogeneity, and then heated in two steps, in the air at 170 °C for 20 h and in the reducing atmosphere (Ar−10% H_2) at 500 °C for 3 h.

The structure of the obtained nanomaterials was checked by X-ray powder diffraction (XRD) using the Rigaku SmartLab device (measurement settings: Cu-K$\alpha_{1,2}$ radiation, λ = 0.1540 nm, ambient temperature, 2θ range 10–90°, measurement step 0.02°, and counting time 1 min/°). Scanning electron images were acquired by a field emission TESCAN MIRA3 microscope. Diffuse spectral reflectance measurements were performed on the FEI TECNAI G2 X-TWIN microscope. Measurements of diffuse reflection spectra were performed on a Thermo Evolution 600 spectrometer equipped with an integrating sphere and using the $BaSO_4$ spectrum as a white standard.

For infrared emission measurements, the sample was pumped by an 808 nm diode laser with about 400 mW output power. The emitted luminescence was collected by a

parabolic mirror and was sent to an FTIR spectrometer (Magna860, Nicodom Ltd., Praha, Czech Republic) equipped with an MCT cooled detector. The resolution of the emission measurements was set to 1 cm^{-1}. All the spectra were corrected for the spectral response of the system using a blackbody source. Lifetimes of excited states were acquired after LED pumping at around 520 nm. The emission was collected by a lens, filtered by suitable filters to cut spurious pump light, and then sent to a fiber-coupled Si detector (OE-200-UV, Femto, Berlin, Germany). The amplification factor of the detector was 10^9 in high-speed mode, so that the response time of the system was 17 µs.

3. Results

XRD patterns shown in Figure 1a confirm that the crystal structures of prepared sesquioxides are cubic bixbyite, space group Ia-3, and for prepared fluoride nanocrystals, it is orthorhombic, space group P_{nma}. No reflections belonging to impurity phases were observed. The average particle sizes of sesquioxides are around 350 nm (Figure 1b) and around 500 nm in fluorides (Figure 1c).
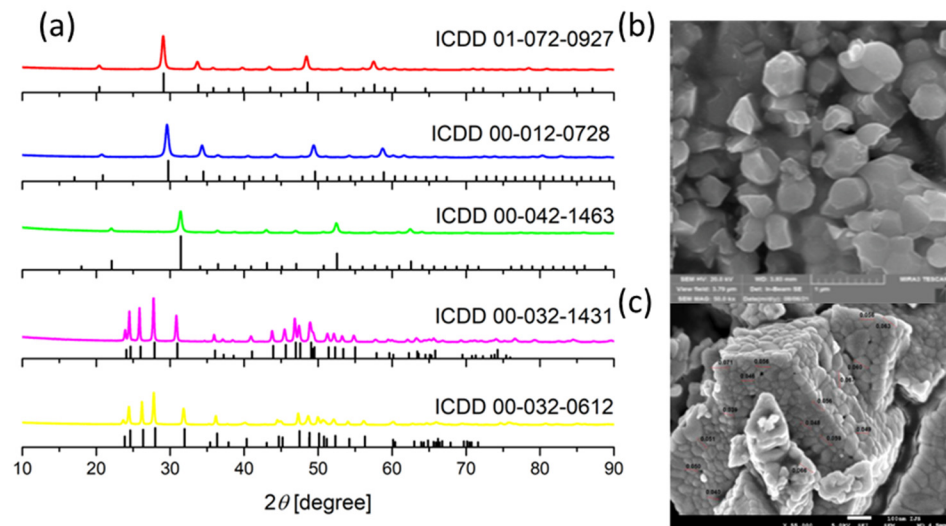
Figure 1. (**a**) XRD patterns of 3%Nd:Y_2O_3, 3%Nd:Lu_2O_3, 3%Nd:Sc_2O_3, 5%Nd:YF_3, and 5%Nd:LuF_3 (top to bottom) with respective ICDD data; (**b**) SEM image of 3%Nd:Y_2O_3; (**c**) SEM image of 5%Nd:YF_3.

3.1. Visible and Near-Infrared Spectroscopy

Diffuse reflection spectra of Nd-doped sesquioxides and fluorides are shown in Figure 2a,b, respectively. Measurements reveal typical absorptions of trivalent Nd located in low-energy phonon hosts, among which the strongest absorption around 800 nm is due to electronic transitions to $^4F_{5/2}$ and $^2H_{9/2}$ from the ground state.
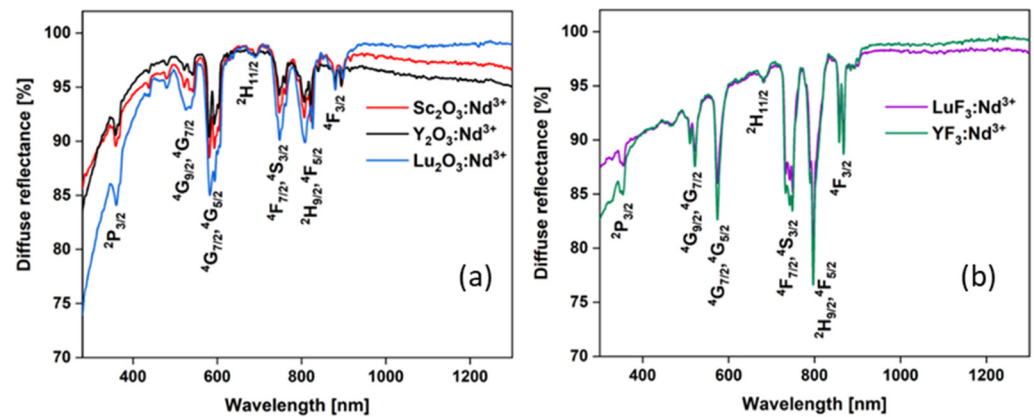
Figure 2. Diffuse reflection spectra of (**a**) 3%Nd:Y_2O_3, 3%Nd:Lu_2O_3, and 3%Nd:Sc_2O_3, and (**b**) 5%Nd:YF_3 and 5%Nd:LuF_3.

3.2. Sesquioxides

All sesquioxide samples show four emission bands that are composed of a series of well-separated peaks, as expected by the strong crystal field of these crystal matrixes [27]. The first band extends from 11,500 cm^{-1} to 10,000 cm^{-1} and corresponds to the $^4F_{3/2}$ → $^4I_{9/2}$ transition, the second extends from 9600 cm^{-1} to 8600 cm^{-1} and corresponds to the $^4F_{3/2}$ → $^4I_{11/2}$ transition, and the third extends from 7800 cm^{-1} to 6700 cm^{-1} and corresponds to the $^4F_{3/2}$ → $^4I_{13/2}$ transition. The peak position agrees with the energy level position reported in the literature [27]. Spectra are very similar among the various compositions. In fact, we can notice a strong similarity in the shape of these emission spectra, with only a small shift of the emission features and small differences in the relative emission intensity among the three compounds. This is not unexpected since Y_2O_3, Sc_2O_3, and Lu_2O_3 are isomorphs. When going from Y_2O_3 to Lu_2O_3 and to Sc_2O_3, the emission features experience a tendency to redshift that is more pronounced for the longest wavelength emission peaks within each band. This can be ascribed to the increasing crystal field strength in the three compounds [20]. The strongest peaks of the first band are located at 10,560 cm^{-1} (947 nm) in Y_2O_3, 10,240 cm^{-1} (977 nm) in Lu_2O_3, and 10,350 cm^{-1} (966 nm) in Sc_2O_3. As usual for Nd-doped compounds, the strongest emission band is the one located at around 1 micron with maxima at 9265 cm^{-1} (1079 nm) for Y_2O_3, 9253 cm^{-1} (1081 nm) for Lu_2O_3, and 9237 cm^{-1} (1083 nm) for Sc_2O_3. The maxima of the 1.3 μm band are located at 7363 cm^{-1} (1358 nm) for Y_2O_3, 7352 cm^{-1} (1360 nm) for Lu_2O_3, and 7311 cm^{-1} (1368 nm) for Sc_2O_3. Moreover, in all cases, we were able to observe a fourth emission band in the 2 μm region that extends from about 4500 cm^{-1} to about 6000 cm^{-1}. This band is usually considered very weak, and the emission has rarely been reported in the literature, even in bulk crystals. As for the other bands, also in this region, the shapes of the spectra look very similar for the three compounds with a tendency to red-shifting when passing from Y_2O_3 to Lu_2O_3 and to Sc_2O_3. The highest peaks are located at 4800 cm^{-1} (2083 nm) for Y_2O_3, 4760 cm^{-1} (2101 nm) for Lu_2O_3, and 4632 cm^{-1} (2159 nm) for Sc_2O_3.

From the emission spectra, we calculated the emission cross-section of the $^4F_{3/2}$ → ^4I_i (i = 9/2, 11/2, 13/2, 15/2) emission bands with the following equation [28]:

$$\sigma_{em}(\nu) = \frac{c^2 I(\nu)}{8\pi\tau n^2 h\nu^3 \int \frac{I(\nu)}{h\nu}d\nu} \tag{1}$$

where *c* is the speed of light in vacuum, *h* is Planck's constant, $I(\nu)$ is the fluorescence signal, and *n* and *τ* are the crystal refractive indexes at 1 μm wavelength and the radiative lifetime, respectively, both taken from the literature as reported in Table 1 for the various compounds. For LuF_3, we could not find proper references to published values; therefore, we used the values of the isomorph compound YF_3. In Equation (1), the integral is over the whole emission region of the $^4F_{3/2}$ decay channels, including the 2 μm emission band.

It is worth mentioning that we performed all the calculations in the frequency domain using Equation (1), because the experimental data were acquired with an FTIR that works at fixed wavenumber intervals, instead of using the equivalent expression in wavelength, as reported in Equation (14) of ref [28] that must be used when working with grating spectrometers.

Table 1. Parameters used for cross-section calculation.

Compound	n	Ref.	τ (µs)	Ref.
Nd:Y_2O_3	1.90	[29]	318	[18]
Nd:Lu_2O_3	1.91	[30]	300	[31]
Nd:Sc_2O_3	1.97	[32]	230	[33]
Nd:YF_3	1.45	[34]	783	[35]

Figure 3a–c show the emission cross-sections of all the Nd-doped sesquioxides in the 11,500 cm^{-1}–6500 cm^{-1} region measured at 1%Nd doping level for oxides and 5%Nd doping level for fluorides because these were the samples with the highest emission intensities. In this region, we can distinguish the three main emission bands. The shape and peak position of the various bands qualitatively agree with published results, when available, and the cross-section peak intensities we obtained are compared with the literature results in Tables 2–6. It is evident that large discrepancies are present among the literature results, especially for the most studied of these compounds, such as Nd:Y_2O_3, where many different estimates are present. Our results compare well with the variation interval of published values. In all cases, the highest emission cross-section is that of the $^4F_{3/2} \rightarrow {}^4I_{11/2}$ transition, and our calculations for this band are in good agreement with published results. The emission cross-section of the other decay channels is not always known in the literature, and when present, our results compare well with published values.

It may be worth noting that these results are similar or slightly lower than the emission cross-section of well-known laser crystals. For example, the maximum emission cross-section of YLF is about 2×10^{-20}, 18×10^{-20}, and 3×10^{-20} cm^2 for the $^4F_{3/2} \rightarrow {}^4I_{9/2}$, $^4F_{3/2} \rightarrow {}^4I_{11/2}$, and $^4F_{3/2} \rightarrow {}^4I_{13/2}$ transitions, respectively [36].

Table 2. Emission cross-sections of Nd:Y_2O_3.

	Decay Channel	σ_{em} (10^{-20} cm^2)						
	$^4F_{3/2} \rightarrow$	This work	[14]	[18]	[16]	[15]	[17]	[13]
Nd:Y_2O_3	$^4I_{9/2}$	2.4	-	-	-	-	4.89	1.8
	$^4I_{11/2}$	7.3	6.9	1.73	7.24	5.13	6.35	6.8
	$^4I_{13/2}$	1.5	5.5	-	-	-	0.92	-
	$^4I_{15/2}$	0.07	-	-	-	-	-	-

Table 3. Emission cross-sections of Nd:Lu_2O_3.

	Decay Channel	σ_{em} (10^{-20} cm^2)				
	$^4F_{3/2} \rightarrow$	This work	[20]	[21]	[27]	[37]
Nd:Lu_2O_3	$^4I_{9/2}$	2.4	-	-	1.9	-
	$^4I_{11/2}$	5.9	8.49	6.5	5.0	6.5
	$^4I_{13/2}$	1.3	-	-	3.1	-
	$^4I_{15/2}$	0.04	-	-	-	-
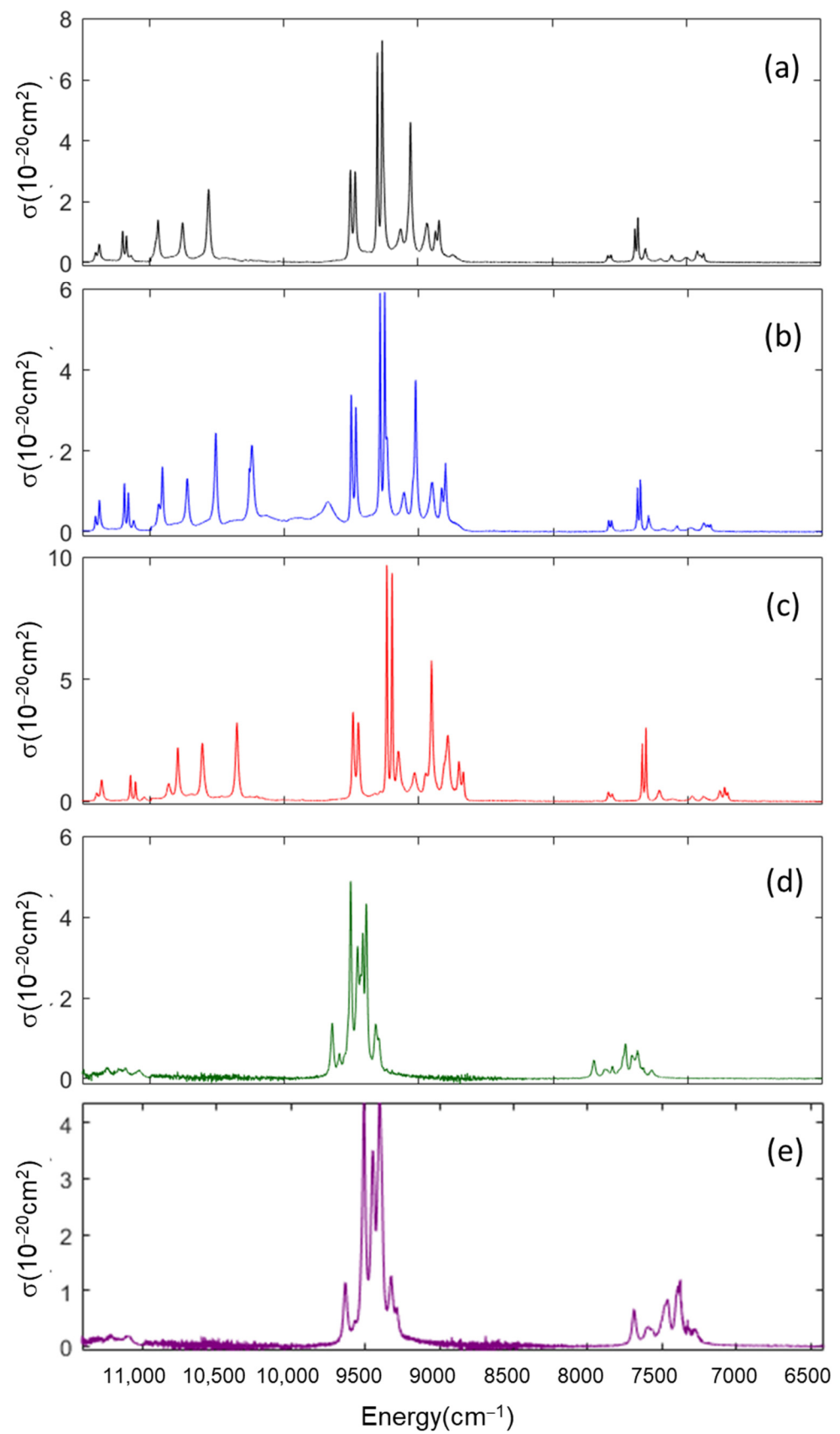
Figure 3. Emission cross-section of the various samples in the 6000–12,000 cm^{-1} range: (**a**) 1%Nd:Y$_2$O$_3$; (**b**) 1%Nd:Lu$_2$O$_3$; (**c**) 1%Nd:Sc$_2$O$_3$; (**d**) 5%Nd:YF$_3$; (**e**) 5%Nd:LuF$_3$.

Table 4. Emission cross-sections of Nd:Sc$_2$O$_3$.

	Decay Channel		σ_{em} (10^{-20} cm^2)	
	$^4F_{3/2} \rightarrow$	This work	[33]
Nd:Sc$_2$O$_3$	$^4I_{9/2}$	3.2	-
	$^4I_{11/2}$	9.7	9.5
	$^4I_{13/2}$	3	-
	$^4I_{15/2}$	0.09	-

Table 5. Emission cross-sections of Nd:YF$_3$.

	Decay Channel		σ_{em} (10^{-20} cm^2)	
	$^4F_{3/2} \rightarrow$	This work	[35] *
Nd:YF$_3$	$^4I_{9/2}$	0.3	0.51
	$^4I_{11/2}$	4.9	0.74
	$^4I_{13/2}$	0.9	0.4
	$^4I_{15/2}$	0.06	0.032

* calculated.

Table 6. Emission cross-sections of Nd:LuF$_3$.

	Decay Channel	σ_{em} (10^{-20} cm^2)
	$^4F_{3/2} \rightarrow$	This work
Nd:LuF$_3$	$^4I_{9/2}$	0.2
	$^4I_{11/2}$	4.7
	$^4I_{13/2}$	1.1
	$^4I_{15/2}$	0.1

The stimulated emission cross-section for the $^4F_{3/2} \rightarrow ^4I_{15/2}$ decay is depicted in Figure 4a–c for all investigated compounds. This transition appears as a series of separated groups of peaks of increasing intensity. The highest emission cross-section is observed at around 2.1 μm in all compounds.

We also measured the $^4F_{3/2}$ decay time under LED pumping on 3% and 1% doped samples. The decay profile is always exponential and lifetime values measured on 1% doped samples are reported in Tables 7–9 and compared with the literature values on low concentration samples, whenever available. On higher doped samples, concentration quenching effects make the lifetime shorter than the radiative value; we measured 217 μs, 211 μs, and 324 μs in 3%Nd-doped Y$_2$O$_3$, Lu$_2$O$_3$, and Sc$_2$O$_3$, respectively. The product of quantum efficiency and the dopant concentration can be considered as a figure of merit of the material [17]. In the case of 3%Nd:Y$_2$O$_3$, for example, considering a radiative lifetime of 354 μs, this value is 1.8, about 2.7 times higher than that obtained by Kumar and co-workers for the same doping level [17] from which laser emission has been obtained. The values obtained for the other compounds at 3% doping level are 1.8 for Lu$_2$O$_3$ and 2.8 for Sc$_2$O$_3$.
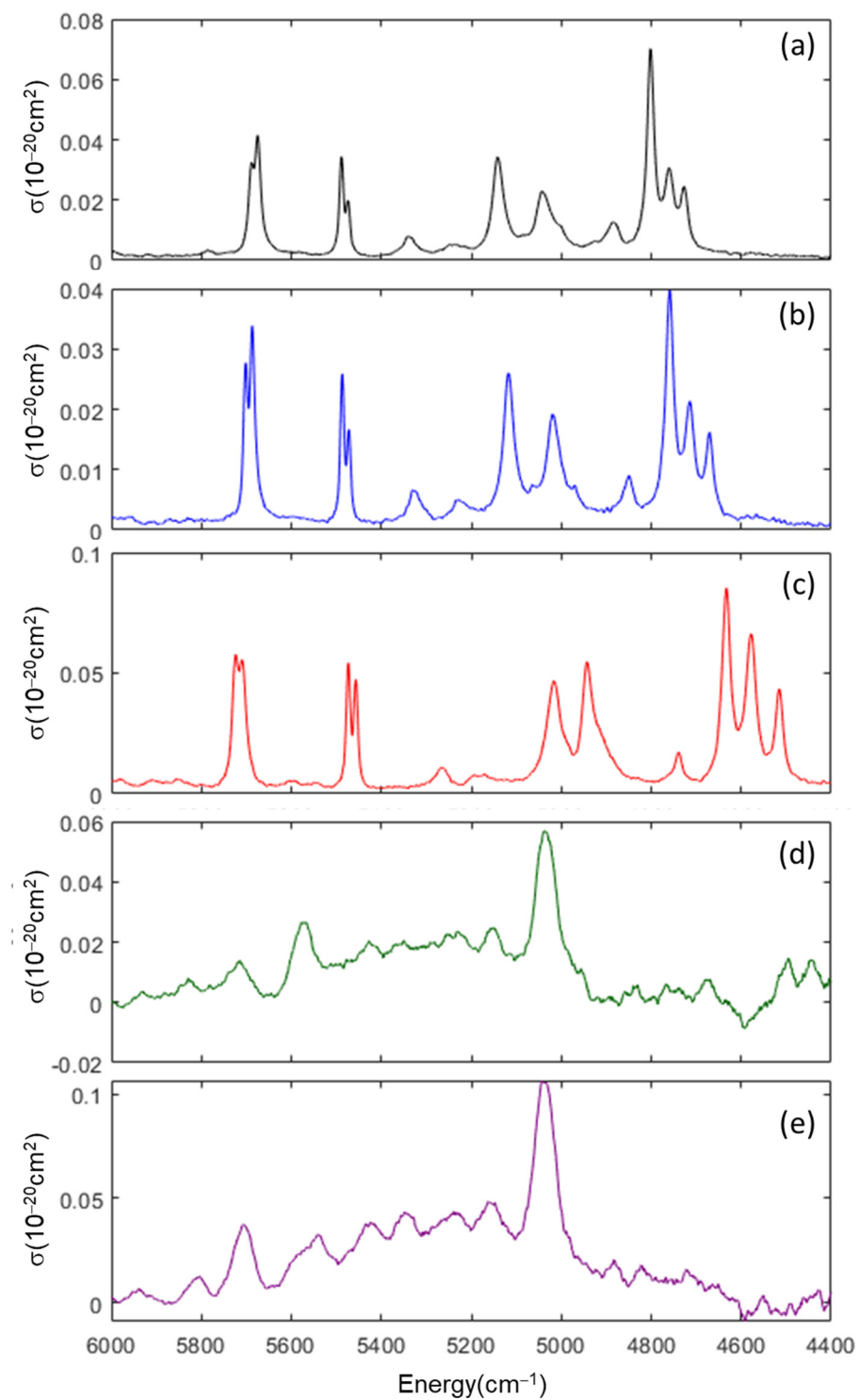
Figure 4. Emission cross-section of the various samples in the 4400–6000 cm^{-1} range: (**a**) 1%Nd:Y$_2$O$_3$; (**b**) 1%Nd:Lu$_2$O$_3$; (**c**) 1%Nd:Sc$_2$O$_3$; (**d**) 5%Nd:YF$_3$; (**e**) 5%Nd:LuF$_3$.

Table 7. Decay time of 1%Nd:Y$_2$O$_3$.

		This work	[13]	[18]	[16]	[15]	[14]	[17]
					τ (µs)			
Nd:Y$_2$O$_3$		320	300		321	232	340	315
	Radiative		378	318	322			354

Table 8. Decay time of 1%Nd:Lu$_2$O$_3$.

		This work	[20]	[31]	[38]
				τ (μs)	
Nd:Lu$_2$O$_3$		420	286	300	
	Radiative		344		165

Table 9. Decay time of 1%Nd:Sc$_2$O$_3$.

		This work	[33]	[39]	[40]
				τ (μs)	
Nd:Sc$_2$O$_3$		335	180	224	260
	Radiative		344		

For Sc$_2$O$_3$, we investigated the dependence of the emission intensity and of the lifetime as a function of the doping level from 0.5% to 7%. The results are shown in Figure 5. As expected, both the emission intensity and the lifetime decrease with the concentration. The low-doping level value of the lifetime is slightly lower, but consistent with the theoretical radiative lifetime reported in Table 1, but the high concentration values are typically much longer than those measured in Y$_2$O$_3$ with similar doping levels. These results indicate that concentration quenching in Sc$_2$O$_3$ is not very strong and confirm the high quality of our samples.
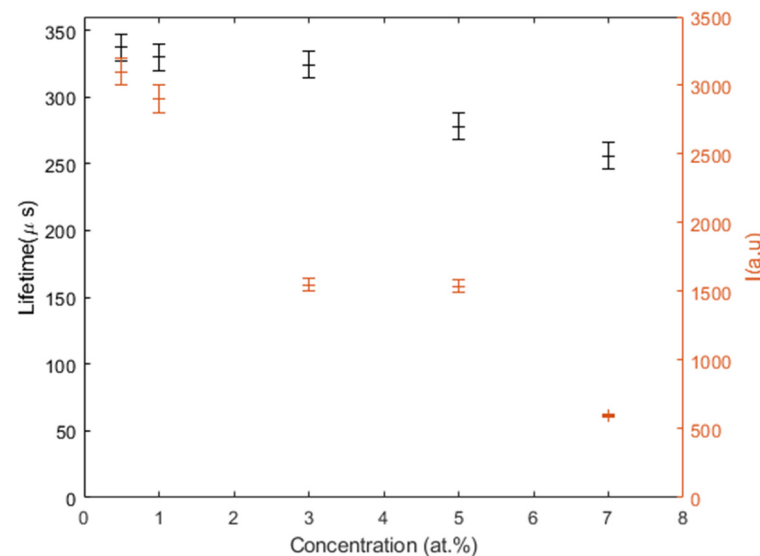
Figure 5. Lifetime of Nd:Sc$_2$O$_3$ (black, left axis) and emission intensity (right, red axis) as a function of the doping level.

3.3. Fluorides

We also acquired the emission spectra from 5%Nd:YF$_3$ and 5%Nd:LuF$_3$ samples and calculated the emission cross-section with Equation (1), as for sesquioxides. Results are shown in Figure 3d,e for the 11,500 cm^{-1}–6500 cm^{-1} region and in Figure 4d,e for the 6000 cm^{-1}–4000 cm^{-1} region. Since the decay time of LuF$_3$ is not known in the literature, the value for YF$_3$ has been used, instead. The emission intensity of fluoride samples is, in general, much weaker than that of sesquioxide samples. This can be ascribed either to the higher Nd doping level of our fluoride samples that can cause concentration quenching effects, or to a worse matching of the emission wavelength of our pump diode that causes lower absorption. In all cases, the emission is dominated by the 1-micron band. The emission cross-sections of the two compounds have similar shapes and intensity, as

expected from the fact that the two compounds are isomorphs, and are much different from that of sesquioxides. The Stark splitting of the energy levels is in general smaller, and single peaks usually merge into continuous bands. The maximum emission cross-section recorded in the 1 μm region is 5×10^{-20} cm^2 and 4.7×10^{-20} cm^2 for YF$_3$ and LuF$_3$, respectively. The emission cross-section in the 2-micron region follows the same features already described: the shape is very similar between FY$_3$ and LuF$_3$ and is composed of an almost featureless band with a few peaks with maximum intensity of about 1×10^{-21} cm^2.

Emission lifetimes of the $^4F_{3/2}$ level have been recorded under LED pumping, and results are reported in Tables 10 and 11 and compared with the literature for YF$_3$. Measured decay times are 170 μs and 120 μs for YF$_3$ and LuF$_3$, respectively. If compared to the radiative lifetime of YF$_3$ of 783 μs determined in [35], we can observe that concentration quenching at this high doping level is strong.

Table 10. Decay time of Nd:YF$_3$.

		τ (μs)	
		This work	[35]
Nd:YF$_3$	5%	169	
	Low C		588
	Radiative		783

Table 11. Decay time of Nd:LuF$_3$.

		τ (μs)
		This work
Nd:LuF$_3$	5%	119

These results show that fluoride materials generally show broader and weaker emission features in all wavelength regions, although fluoride crystals have lower phonon energy. This is probably due to the longer radiative lifetime of fluoride materials, but we cannot rule out interaction with possible quenching centers that are known to severely affect the emission efficiency of lanthanide-doped fluoride materials. The highest emission cross-sections are obtained from Nd:Sc$_2$O$_3$ in all regions.

4. Conclusions

We have synthesized and characterized a set of different Nd-doped fluoride and oxide nanocrystals, namely Nd:Y$_2$O$_3$, Nd:Lu$_2$O$_3$, Nd:Sc$_2$O$_3$, Nd:YF$_3$, and Nd:LuF$_3$. Under 808 nm pumping, we observed the three main emission bands in the near-infrared region, and we measured the lifetime of the $^4F_{3/2}$ level under LED pumping. In all cases, we were able to detect the weak 2-micron emission from the $^4F_{3/2} \rightarrow {}^4I_{15/2}$. Using the emission and lifetime data, we calculated the emission cross-sections of the various emission bands for all the compounds. Oxide materials generally showed narrower emissions, higher emission cross-sections, and shorter lifetimes. The results are in good agreement with the literature data, whenever available.

Author Contributions: Conceptualization, A.T. and M.D.D.; methodology, A.T., Ž.A. and M.D.D.; investigation, F.G., M.S. and T.B.; data curation, F.G.; writing—original draft preparation, F.G.; writing—review and editing, A.T. and M.D.D.; supervision, A.T. and M.D.D.; funding acquisition, M.D.D. All authors have read and agreed to the published version of the manuscript.

Institutional Review Board Statement: Not applicable.

Informed Consent Statement: Not applicable.

Data Availability Statement: All data will be available on request.

Conflicts of Interest: The authors declare no conflict of interest.

References

1. Bouzigues, C.; Gacoin, T.; Alexandrou, A. Biological applications of rare-earth based nanoparticles. *ACS Nano* **2011**, *5*, 8488–8505. [CrossRef]
2. Lim, X. The nanolight revolution is coming. *Nature* **2016**, *531*, 26–28. [CrossRef] [PubMed]
3. Yang, M.; Liang, Y.; Gui, Q.; Zhao, B.; Jin, D.; Lin, M.; Yan, L.; You, H.; Dai, L.; Liu, Y. Multifunctional luminescent nanomaterials from $NaLa(MoO_4)_2$:Eu^{3+}/Tb^{3+} with tunable decay lifetimes, emission colors and enhanced cell viability. *Sci. Rep.* **2015**, *5*, 11844. [CrossRef] [PubMed]
4. Jaque, D.; Vetrone, F. Luminescence nanothermometry. *Nanoscale* **2012**, *4*, 4301. [CrossRef]
5. Dramićanin, M.D. Sensing temperature via downshifting emissions of lanthanide-doped metal oxides and salts. A review. *Methods Appl. Fluoresc.* **2016**, *4*, 042001. [CrossRef]
6. Blumenthal, T.; Meruga, J.; Stanley May, P.; Kellar, J.; Cross, W.; Ankireddy, K.; Vunnam, S.; Luu, Q.N. Patterned direct-write and screen-printing of NIR-to-visible upconverting inks for security applications. *Nanotechnology* **2012**, *23*, 185305. [CrossRef]
7. Cornacchia, F.; Toncelli, A.; Tonelli, M. 2-μm lasers with fluoride crystals: Research and development. *Prog. Quantum Electron.* **2009**, *33*, 61–109. [CrossRef]
8. Zhao, J.; Zhong, D.; Zhou, S. NIR-I-to-NIR-II fluorescent nanomaterials for biomedical imaging and cancer therapy. *J. Mater. Chem. B* **2018**, *6*, 349–365. [CrossRef]
9. Qu, Z.; Shen, J.; Li, Q.; Xu, F.; Wang, F.; Zhang, X.; Fan, C. Near-IR emissive rare-earth nanocrystals for guided surgery. *Theranostics* **2020**, *10*, 2631–2644. [CrossRef] [PubMed]
10. Gee, W.J. Recent trends concerning upconversion nanoparticles and near-IR emissive lanthanide materials in the context of forensic applications. *Aust. J. Chem.* **2019**, *72*, 164. [CrossRef]
11. Denker, B.; Shklovsky, E. (Eds.) *Handbook of Solid-State Lasers: Materials, Systems and Applications*; Woodhead Publishing Series in Electronic and Optical Materials; Elsevier: Amsterdam, The Netherlands, 2013; ISBN 9780857092724.
12. Toncelli, A.; Xu, J.; Tredicucci, A.; Heuer, A.M.; Kränkel, C. Mid-infrared spectroscopic characterization of Pr^{3+}:Lu_2O_3. *Opt. Mater. Express* **2019**, *9*, 4464. [CrossRef]
13. Walsh, B.M.; McMahon, J.M.; Edwards, W.C.; Barnes, N.P.; Equall, R.W.; Hutcheson, R.L. Spectroscopic characterization of Nd:Y_2O_3: Application toward a differential absorption lidar system for remote sensing of ozone. *J. Opt. Soc. Am. B* **2002**, *19*, 2893. [CrossRef]
14. Stone, J.; Burrus, C.A. Nd: Y_2O_3 single-crystal fiber laser: Room-temperature cw operation at 1.07- and 1.35-μm wavelength. *J. Appl. Phys.* **1978**, *49*, 2281. [CrossRef]
15. Zhang, L.; Huang, Z.; Pan, W. High transparency Nd:Y_2O_3 ceramics prepared with La_2O_3 and ZrO_2 additives. *J. Am. Ceram. Soc.* **2015**, *98*, 824–828. [CrossRef]
16. Hou, X.; Zhou, S.; Jia, T.; Lin, H.; Teng, H. Effect of Nd concentration on structural and optical properties of Nd:Y_2O_3 transparent ceramic. *J. Lumin.* **2011**, *131*, 1953–1958. [CrossRef]
17. Kumar, G.A.; Lu, J.; Kaminskii, A.A.; Ueda, K.-I.; Yagi, H.; Yanagitani, T. Spectroscopic and stimulated emission characteristics of Nd^{3+} in transparent Y_2O_3 ceramics. *IEEE J. Quantum Electron.* **2006**, *42*, 643–650. [CrossRef]
18. Cui, X.; Lu, J.; Gao, C.; Hou, C.; Wei, W.; Peng, B. Luminescence properties of Nd^{3+}-doped Y_2O_3 nanocrystals in organic media. *Appl. Phys. A* **2011**, *103*, 27–32. [CrossRef]
19. Belli Dell'Amico, D.; Biagini, P.; Bongiovanni, G.; Chiaberge, S.; di Giacomo, A.; Labella, L.; Marchetti, F.; Marra, G.; Mura, A.; Quochi, F.; et al. A convenient preparation of nano-powders of Y_2O_3, $Y_3Al_5O_{12}$ and Nd:$Y_3Al_5O_{12}$ and study of the photoluminescent emission properties of the neodymium doped oxide. *Inorg. Chim. Acta* **2018**, *470*, 149–157. [CrossRef]
20. Hao, L.; Wu, K.; Cong, H.; Yu, H.; Zhang, H.; Wang, Z.; Wang, J. Spectroscopy and laser performance of Nd:Lu_2O_3 crystal. *Opt. Express* **2011**, *19*, 17774. [CrossRef] [PubMed]
21. Liu, Z.; Toci, G.; Pirri, A.; Patrizi, B.; Feng, Y.; Chen, X.; Hu, D.; Tian, F.; Wu, L.; Vannini, M.; et al. Fabrication and optical property of Nd:Lu_2O_3 transparent ceramics for solid-state laser applications. *J. Inorg. Mater.* **2021**, *36*, 210. [CrossRef]
22. Wang, Y.; Lu, B.; Sun, X.; Sun, T.; Xu, H. Synthesis of nanocrystalline Sc_2O_3 powder and fabrication of transparent Sc_2O_3 ceramics. *Adv. Appl. Ceram.* **2011**, *110*, 95–98. [CrossRef]
23. Ubaldini, A.; Carnasciali, M.M. Raman characterisation of powder of cubic RE_2O_3 (RE = Nd, Gd, Dy, Tm, and Lu), Sc_2O_3 and Y_2O_3. *J. Alloys Compd.* **2008**, *454*, 374–378. [CrossRef]
24. Lojpur, V.M.; Ahrenkiel, P.S.; Dramićanin, M.D. Color-tunable up-conversion emission in Y_2O_3:Yb^{3+}, Er^{3+} nanocrystals prepared by polymer complex solution method. *Nanoscale Res. Lett.* **2013**, *8*, 131. [CrossRef]
25. Krsmanović, R.; Antić, Ž.; Bártová, B.; Dramićanin, M.D. Characterization of rare-earth doped Lu_2O_3 nanopowders prepared with polymer complex solution synthesis. *J. Alloys Compd.* **2010**, *505*, 224–228. [CrossRef]
26. Ćirić, A.; Aleksić, J.; Barudžija, T.; Antić, Ž.; Đorđević, V.; Medić, M.; Periša, J.; Zeković, I.; Mitrić, M.; Dramićanin, M.D. Comparison of three ratiometric temperature readings from the Er^{3+} up-conversion emission. *Nanomaterials* **2020**, *10*, 627. [CrossRef] [PubMed]

27. Chang, N.C. Energy levels and crystal-field splittings of Nd $^{3+}$ in yttrium oxide. *J. Chem. Phys.* **1966**, *44*, 4044–4050. [CrossRef]

28. Aull, B.; Jenssen, H. Vibronic interactions in Nd:YAG resulting in nonreciprocity of absorption and stimulated emission cross sections. *IEEE J. Quantum Electron.* **1982**, *18*, 925–930. [CrossRef]

29. Nigara, Y. Measurement of the optical constants of yttrium oxide. *Jpn. J. Appl. Phys.* **1968**, *7*, 404–408. [CrossRef]

30. Medenbach, O.; Dettmar, D.; Shannon, R.D.; Fischer, R.X.; Yen, W.M. Refractive index and optical dispersion of rare earth oxides using a small-prism technique. *J. Opt. A Pure Appl. Opt.* **2001**, *3*, 174–177. [CrossRef]

31. Von Brunn, P.; Heuer, A.M.; Fornasiero, L.; Huber, G.; Kränkel, C. Efficient laser operation of Nd^{3+}:Lu_2O_3 at various wavelengths between 917 nm and 1463 nm. *Laser Phys.* **2016**, *26*, 084003. [CrossRef]

32. Belosludtsev, A.; Juškevičius, K.; Ceizaris, L.; Samuilovas, R.; Stanionytė, S.; Jasulaitienė, V.; Kičas, S. Correlation between stoichiometry and properties of scandium oxide films prepared by reactive magnetron sputtering. *Appl. Surf. Sci.* **2018**, *427*, 312–318. [CrossRef]

33. Kuzminykh, Y.; Kahn, A.; Huber, G. Nd^{3+} doped Sc_2O_3 waveguiding film produced by pulsed laser deposition. *Opt. Mater.* **2006**, *28*, 883–887. [CrossRef]

34. Barnes, N.P.; Gettemy, D.J. Temperature variation of the refractive indices of yttrium lithium fluoride. *J. Opt. Soc. Am.* **1980**, *70*, 1244–1247. [CrossRef]

35. Tan, M.C.; Kumar, G.A.; Riman, R.E.; Brik, M.G.; Brown, E.; Hommerich, U. Synthesis and optical properties of infrared-emitting YF_3:Nd nanocrystals. *J. Appl. Phys.* **2009**, *106*, 063118. [CrossRef]

36. Turri, G.; Webster, S.; Bass, M.; Toncelli, A. Temperature-dependent stimulated emission cross-section in Nd^{3+}:YLF crystal. *Materials* **2021**, *14*, 431. [CrossRef]

37. Zhou, D.; Shi, Y.; Xie, J.; Ren, Y.; Yun, P. Fabrication and luminescent properties of Nd^{3+}-doped Lu_2O_3 transparent ceramics by pressureless sintering. *J. Am. Ceram. Soc.* **2009**, *92*, 2182–2187. [CrossRef]

38. Zhou, D.; Cheng, Y.; Ren, Y.Y.; Shi, Y.; Xie, J.J. Fabrication and spectroscopic properties of Nd:Lu_2O_3 transparent ceramics for laser media. In *Ceramic Materials and Components for Energy and Environmental Applications*; Jiang, D., Zeng, Y., Singh, M., Heinrich, J., Eds.; Ceramic Transactions Series; John Wiley & Sons, Inc.: Hoboken, NJ, USA, 2010; pp. 605–610. ISBN 978-0-470-64084-5.

39. Fornasiero, L.; Mix, E.; Peters, V.; Heumann, E.; Petermann, K.; Huber, G. *Advanced Solid-State Lasers*; OSA Trend in Optics and Photonics Series; Optical Society of America: Washington, DC, USA, 1999; Volume 26, p. 249.

40. Zverev, G.M.; Kolodnyi, G.Y.; Smirnov, A.I. Optical spectra of Nd^{3+} in single crystals of scandium and yttrium oxides. *Opt. Spectrosc.* **1967**, *23*, 325–327.